A virtual test rig for performance and efficiency assessment of heat pump thermal management system for battery electric vehicles

Applied Thermal Engineering 247 (2024) 123055

Contents lists available at ScienceDirect

Applied Thermal Engineering

journal homepage: www.elsevier.com/locate/apthermeng

Research Paper

A virtual test rig for performance and efficiency assessment of heat pump thermal management system for battery electric vehicles

Luciano Rolando [a], Federico Millo [a], Afanasie Vinogradov [a], Benedetta Peiretti Paradisi [a,*], Alessandro Allocco [b], Pasquale Ceres [b], Rossella Marco [b], Matteo Maria Rostagno [b]

[a] Energy Department, Politecnico di Torino, Corso Duca degli Abruzzi 24, 10129 Torino, Italy
[b] Centro Ricerche Fiat S.p.A., Orbassano, Italy

ARTICLE INFO

Keywords:
Thermal management
Battery electric vehicles
Digital twin
Heat pump system

ABSTRACT

In a Battery Electric Vehicle (BEV), the optimization of its thermal state plays a crucial role in the achievement of relevant vehicle targets such as range, passenger comfort, and recharging times, as well as varying external ambient conditions. Therefore, selecting the most proper solution between the many possible architectures to manage the different thermal loads of a BEV needs the support of a robust simulation platform. In such a framework, a comprehensive numerical twin of an electric city car was developed in the GT-Suite environment and validated against experimental data. Through that, the promising performance of a Heat Pump (HP) based thermal layout has been demonstrated, against a standard Air Conditioning system integrated with a PTC heater, on a wide range of external ambient temperatures (reaching up to +20 % driving range improvement in cold conditions). The present layout proposed a sustainable alternative to the most common R134a as working fluid (i.e., propane) and the integration of multiple heat sources. In addition, different battery preconditioning strategies have been tested, tailored to the selected real-world mission profiles, obtaining a remarkable gain in terms of driving range for the HP system in cold conditions (up to 6 % at −10 °C and 4 % at −20 °C).

1. Introduction

Nowadays, extremely demanding environmental legislation requirements and vehicle purchase incentives force the adoption of Electric Vehicles (EVs) to limit local tailpipe emissions [1], confirming the actual growth of EVs sales in 2023. Despite of this trend, limited range and long battery charging time are key consumer concerns that restrain Battery Electric Vehicles (BEVs) mass adoption [2]. Moreover, the performance of BEVs is strongly affected by adverse weather conditions, where high demand for cabin conditioning and reduced capacity of the battery decrease the electrical energy available for vehicle propulsion, shortening the driving range [3]. Indeed, an operating temperature between 10 and 35 °C for a Li-Ion battery is required to maintain nominal capacity, maximum power, and durability [4], and to avoid thermal runaway phenomena produced by cell overheating [5]. Last, but not least, unlike conventional Internal Combustion Engines (ICEs) based vehicles, in BEVs, very limited waste heat is available to be reused in cold climates and most of the heat needed is commonly generated by electric heaters, such as Positive Temperature Coefficient (PTC) devices [6]. Their advantages are low cost, easy installation, and quick transient response; nevertheless, the provided heat is produced directly from electricity, becoming one of the main energy consumers of the vehicle and in turn eroding the range. As an example, the combination of cabin heating by PTC and higher battery charge transfer resistance at low temperatures could give a range loss of up to 50 % [7].

On this basis, the interest in advanced Thermal Management Systems (TMSs) able to ensure the optimal battery operating temperature and cabin thermal comfort, with minimum penalties on the driving range is growing [8]. Among the investigated solutions, Heat Pump (HP) systems represent one of the most promising, as demonstrated by their implementation in a wide range of EVs already available in the market (e.g., Nissan Leaf, Volkswagen IDp3 or Tesla Model Y [9–11]). In particular, HPs can provide both heating and cooling capacity, depending on the external ambient temperature, with a power consumption of about one-third of an electric PTC system for the same heating capacity [12] and reaching a Coefficient of Performance (COP) higher than 1 [13]. However, even if the vehicle is equipped with an HP, cold climate conditions

* Corresponding author.
E-mail addresses: luciano.rolando@polito.it (L. Rolando), federico.millo@polito.it (F. Millo), afanasie.vinogradov@polito.it (A. Vinogradov), benedetta.peiretti@polito.it (B. Peiretti Paradisi), alessandro.allocco@crf.it (A. Allocco), pasquale.ceres@crf.it (P. Ceres), rossella.marco@crf.it (R. Marco), matteo.rostagno@crf.it (M.M. Rostagno).

https://doi.org/10.1016/j.applthermaleng.2024.123055
Received 8 December 2023; Received in revised form 26 February 2024; Accepted 27 March 2024
Available online 28 March 2024

Nomenclature

Definitions/Abbreviations

1D-CFD	One Dimensional Computational Fluid Dynamics
AC	Air Conditioning
BEV	Battery Electric Vehicle
COP	Coefficient of Performance
CO_2	Carbon Dioxide
CRU	Compact Refrigeration Unit
EV	Electric Vehicle
GWP	Global Warming Potential
HP	Heat Pump
ICE	Internal Combustion Engine
PCM	Phase Change Material
PID	Proportional Integrative Derivative
PTC	Positive Temperature Coefficient
PWT	Powertrain
RDE	Real Driving Emissions
SOC	State of Charge
TMS	Thermal Management System
WLTC	World-wide harmonized Light-duty vehicles Test Cycle

Symbols

Q	Thermal load provided by the heat pump
W	Work needed to move the HP refrigerant

remain challenging: indeed, the lower the external temperature, the lower the COP [14]. A solution for a partial efficiency improvement could be the exploitation of multiple heat sources, such as waste heat from electric devices (i.e., electric motor, inverter) [15] and from the battery [16]. Other strategies could further improve HP system performance, such as a gas injection cycle for heating capacity increase [7], the introduction of Phase Change Material (PCM) heat exchangers as thermal storage [17,18], or thermoelectric heaters [19]. Nevertheless, these technologies are still not mature for the real market, or commercially available. In addition, another critical aspect is the refrigerant implemented in the vapor compression cycle. At present, in the automotive sector, the dominant working fluid is the R134a thanks to its compatibility with a direct circuit in the cabin (i.e., low flammability) and its relatively low operating pressure. However, it features a Global Warming Potential (GWP) of 1300 and the European Union advises the progressive phase-out for refrigerants with GWP $>$ 150 in mobile Air Conditioning (AC) systems [20]. Alternative refrigerants, such as hydrocarbon mixtures (e.g., propane), CO_2 and R1234yf have been proposed [21]. Table 1 presents a summary of the fluid properties. Among them, R1234yf is now the mainstream adopted option as a successor in HP units due to its mild flammability and comparable refrigerant characteristics with respect to R134a [22]. Regarding CO_2, good heating performance (i.e., COP $>$ 3) has been demonstrated in cold climates [23], while its diffusion worldwide is limited by poor refrigerant characteristics in hot environments and high working pressure (see Table 1) [24]. R290 (propane) has a very good performance for heating and cooling, with a GWP much lower concerning the imposed limit [25]. Nevertheless, due to its high flammability, it could not be implemented directly for cabin conditioning, and it requires a secondary loop with a safe fluid, which can jeopardize the efficiency benefits [26].

Table 1
Properties of different refrigerants for HP systems.

	R134a	R1234yf	R290	R744 (CO2)
GWP	1430	4	3	1
Flammability	Low	Medium	High	Low
Critical Temperature [°C]	101.1	95.0	96.7	31.1
Critical Pressure [bar]	40.7	33.8	42.5	73.6

All in all, advanced HP configurations seem the most sustainable solution to enhance the driving range of BEVs, thanks to the above-mentioned peculiarities. However, considering the different operating modes of an integrated TMS depending on external conditions and the variety of the BEV subcomponents' thermal requirements, an optimal and comprehensive architecture solution has not been identified [27,28]. In addition, an alternative valuable refrigerant compliant with European directives and with satisfactory thermal properties has not been clearly identified and is still not available in the market [29]. In this context, numerical simulations can represent a viable tool to identify the TMS configuration capable of maximizing the powertrain efficiency, achieving, at the same time, the comfort constraints, and considering HP systems complexity [30]. As a result, the present work aims to develop a physical virtual test rig to support the design of an integrated TMS able to manage the different thermal loads of a BEV, from the cabin to the battery, minimizing the penalties on the driving range and also in extreme external ambient conditions. In particular, a novel HP-based TMS is modeled, featuring propane as a low GWP refrigerant and considering multiple passive heat sources, in addition to the external ambient. Its performances are benchmarked against the ones of a conventional AC system, which features PTC heaters to be used in cold environments, to highlight the advantages of the propane HP system in different ambient conditions.

The main novelties of the proposed system, considered compelling contributions to the existing literature on BEV thermal management, could be summarized as follows:

1. The analysis of a TMS featuring an indirect HP circuit, based on a vapor compressor cycle of propane, as a promising alternative to R134a with a much lower GWP (i.e., one of the first examples in the literature, to the Authors' knowledge).
2. The integration of multiple heat sources in addition to the external ambient to enhance the system efficiency in cold ambient conditions, as the heat that comes from the powertrain.
3. The wide range of environmental conditions and mission profiles tested, including real driving conditions and homologation cycles.
4. The evaluation of the impact on the driving range of different battery preconditioning strategies.

The present paper is organized as follows: first, the test case is described, then the TMS architectures are presented (Section 2). It follows the methodology section with the description of the numerical models and their control strategies, together with the calibration and validation of the virtual test rig against the available experimental data (Section 3). Thereafter, the simulation results are discussed, showing the HP system dynamic and efficiency in extreme hot and cold environments. Then, two different preconditioning strategies are applied, heating the battery before or during the driving cycle depending on the time available for the cruise (Section 4). All the results of the analysis are benchmarked against the ones obtained for a standard PTC system. Finally, the paper summarizes the main findings of the work, highlighting the benefits and limitations of HP-based TMSs (Section 5).

2. Test case

Both HP and standard TMS have been integrated on an A-Class BEV, where the main specifications are reported in Table 2.

2.1. Driving cycles and test conditions

The simulations have been performed on two driving cycles, the World-wide harmonized Light-duty vehicles Test Cycle (WLTC) and a Real Driving Emissions (RDE) cycle [31]. The WLTC can be representative of the declared range and of a short mission profile, while the RDE presented in Fig. 1, evidences the effect of thermal systems on the range

Table 2
Main Specifications of the tested vehicle.

Vehicle Mass [kg]	1450
Rolling Radius [m]	0,3
Top Speed [km/h]	150
Acceleration 0 – 100 km/h [s]	9
Max Transient Mech. Power [kW]	85
Max Transient Torque [Nm]	200
Battery Energy Capacity [kWh]	42

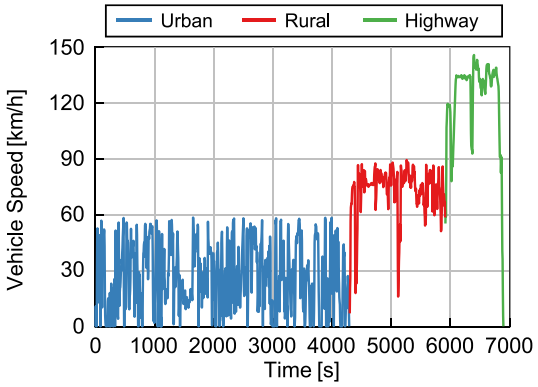

Fig. 1. Speed profile of the RDE with urban, rural, and highway sections evidenced.

in a longer and more aggressive driving cycle.

For both conditions, a wide range of operating conditions was taken into account including extremely hot and cold situations (see Table 3).

2.2. Thermal management systems

In this study, two TMS configurations, integrated in the same vehicle, have been considered. The former uses an indirect HP system operating with R290 (propane) as a refrigerant and EGL 5050 as a secondary liquid, in order to be compliant with the security requirements of the cabin. The latter is a standard air conditioning system, using R134a as refrigerant, combined with two PTC heaters used in cold environments to heat both the battery and the cabin.

The indirect HP system is visible in Fig. 2 and is based on a Compact Refrigeration Unit (CRU), that heat up or cool down the secondary liquid. The CRU is a device that exploits a reverse Rankine cycle: through the electric compressor, the refrigerant is pressurized and heated up, at first, inside the condenser, the external liquid is heated by the refrigerant condensation, then, after the expansion, the cold refrigerant evaporates by cooling down the fluid. The hot (or cold) fluid coming from the CRU is distributed through the secondary loop according to the needs of the cabin and the battery. The management of the secondary fluid is performed by six 3-way valves and by two recirculation pumps at the inlet of the CRU, highlighted in Fig. 2, which distribute the EGL according to the battery and cabin requirements. A third recirculation pump positioned in parallel to the battery loop could be additionally used to achieve the temperature target at the inlet. Then, a radiator is used to dissipate heat generated during the cooling mode and to extract heat from the external environment during HP operations.

Table 3
Considered ambient conditions.

	Hot ambient		**Cold ambient**			
Ambient Temperature [°C]	42	35	5	0	−10	−20
Solar Irradiance [W/m^2]	800	600	0	0	0	0
Air Recirculation Rate [%]	60	60	40	30	30	30

Downstream the radiator, the liquid flows through the powertrain loop circuit. Since the liquid temperature at the radiator outlet is compliant with the electric motor and inverter requirements the liquid could flow in the powertrain loop, if necessary. On the other side, it can be used to recover heat from the powertrain in cold conditions.

The standard TMS is represented in Fig. 3. It also relies on the reverse Rankine cycle, but in this case, the evaporator and condenser directly exchange heat with the cabin air and the underhood, respectively. To cool down the battery, a fraction of the refrigerant is extracted from the AC system and used in a secondary battery chiller, which will cool down the liquid used by the battery coolant loop (represented in yellow in Fig. 3). As already mentioned, both the battery and cabin heating are performed through two PTC heaters. The powertrain, in this case, has its dedicated loop (represented in green in Fig. 3) with a specific radiator in the underhood.

3. Methodology

The virtual test rig of the above-mentioned TMSs was built in the commercial GT-Suite software [32] that relies on a multiphysics approach, crucial to properly reproduce the dynamic of the different vehicle domains (biphasic refrigerant, thermofluid-dynamics, electrical and mechanical). Longitudinal dynamics is used for vehicle speed evaluation with a forward approach [33]. 1D-CFD is adopted to model the cooling flow of the systems described above, as well as the thermo-fluid dynamics of the heat exchangers. Since no detailed specifications were available for the cabin system, a combination of estimated and literature data was employed [32]. The cabin is modeled through several lumped masses that exchange heat with the environment through solar radiation, convection, and conduction and with a cooling system through two liquid-to-air heat exchangers: a chiller and a heater. The air flux inside the cabin is guaranteed by an electric blower, modeled with a 0D approach through a performance map and a regulation flap is used to guarantee the correct level of air recirculation. The positive displacement compressor model uses volumetric and isentropic efficiency to evaluate mass flow rate and pressure rise. The battery is modeled with a Thevenin equivalent circuit, as represented in Fig. 4, in which OCV and internal resistance are obtained by the interpolation of experimental maps depending on temperatures and SOC [34]. At the same time, charging and discharging current limitations of the battery are dependent on the temperature and the SOC. The effect will directly influence the regenerative braking potential. In the end, the dependency on temperature is fundamental to couple the electrical and thermal domains. From this perspective, the thermal inertia of the battery is modeled with multiple lumped masses, with the aim of catching possible uneven heating. More in detail 6 nodes were used, 3 for each battery module. As depicted in Fig. 4, the top side exchanges heat with the cabin, but the major heat extraction is coming from the bottom side, in contact with the coolant. The heat produced through the Joule effect is uniformly distributed among the lumped masses, thermally connected. Finally, the battery can also exchange heat with the cabin and cooling fluid through convection.

A similar approach is used for the inverter and the electric motor thermal model: where the power losses are converted into heat and dissipated towards a thermal lumped mass which exchanges convective heat with a coolant fluid flowing into a pipe. To control both the cabin and battery temperatures a Proportional Integrative Derivative (PID) controller acts on the compressor speed. A ruled-based approach dependent on the difference between the cabin target temperature and the external temperature was used to control the opening configuration of the 6 three-way valves. The different configurations of the valve can be switched based on the request of the cabin or battery conditioning system. In the end, the radiator fan speed is controlled through an empirical relationship dependent on propane pressure and temperature.

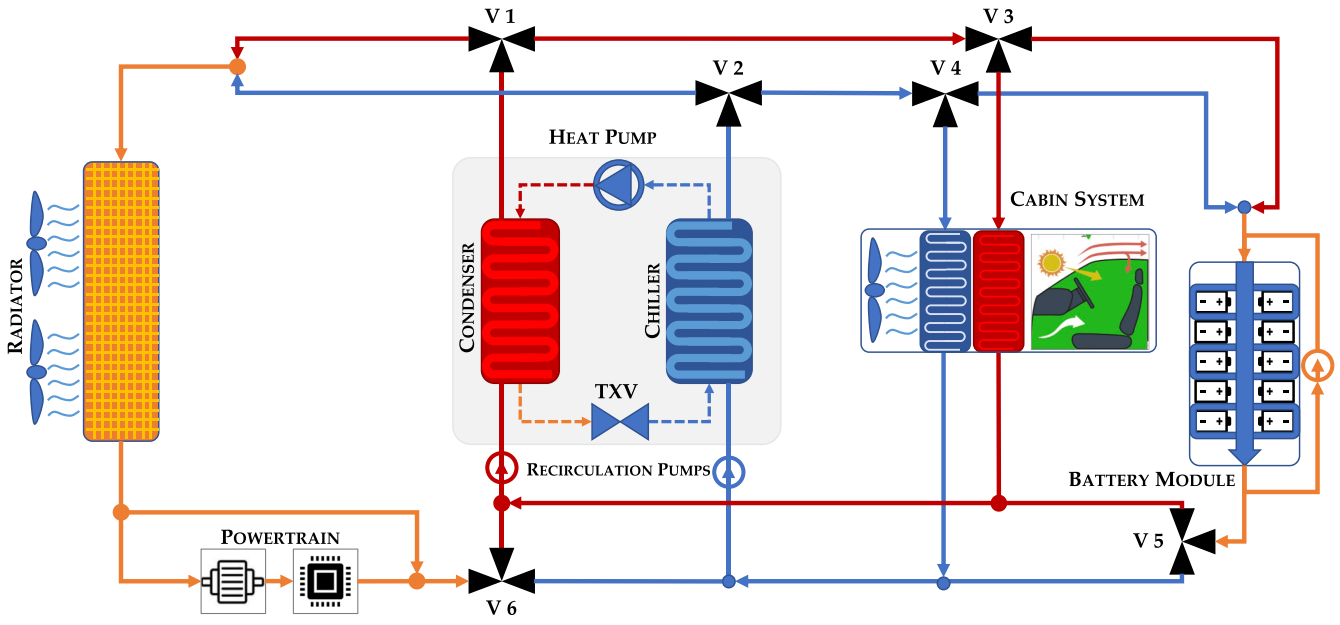

Fig. 2. Scheme of the TMS based on the HP.

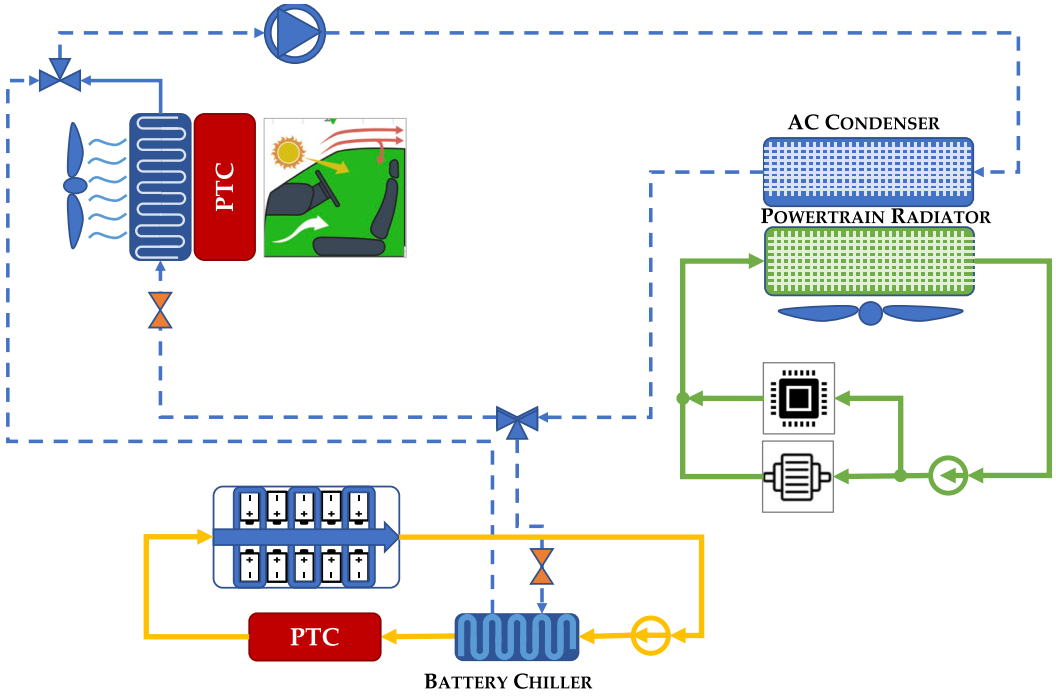

Fig. 3. Scheme of the standard TMS, featuring an AC system and two PTC heaters.

3.1. Model calibration and validation

The model calibration and validation of the HP TMS were performed by exploiting a set of data measured on a similar vehicle configuration in [35], under hot external conditions, on a sequence of WLTC driving cycles. The CRU was calibrated by imposing boundary conditions, in terms of ambient conditions and driving cycle, and then performance maps of the compressor were scaled from literature data [36], together with the heat transfer multiplier adjusted for the heat exchangers. Some results of the calibration process are represented in Fig. 5. The simulated compressor power (Fig. 5a), which represents the highest energetic demand of the thermal system, is properly matched with the experimental data along the whole cycle. Satisfactory results were obtained for the propane temperatures inside the CRU (Fig. 5b), showing a good agreement with experimental data especially in the steady part of the cycle, where the maximum error is about 4 °C degree. On the other side, the higher dynamic of the simulated temperature is probably related to the lack of a thermocouple model. The cabin temperature shows a good match both in the transient and steady-state part of the cycle (Fig. 5c), with a maximum error lower than 1 °C degree, indicating that the thermal load is well predicted. Finally, it can be stated that battery inertia was properly set since all simulated temperature variations are consistent with the experimental data with a max 0.5° C degree of error (Fig. 5d). The model has been also further validated in cold

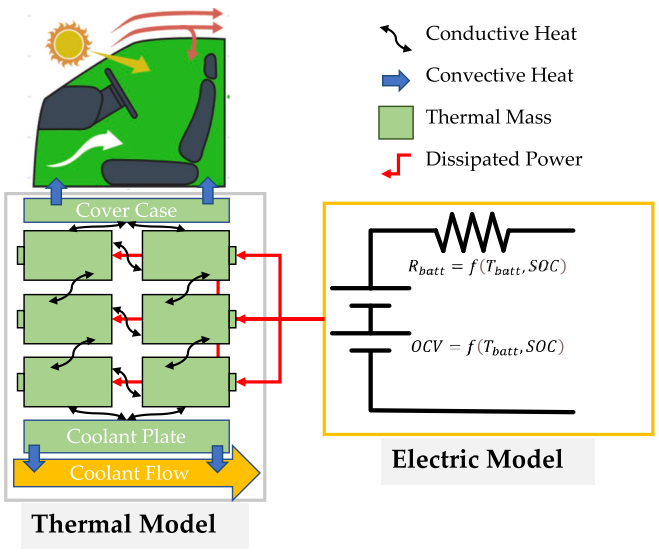

Fig. 4. Scheme of the battery thermal and electrical coupling inside the simulation tool.

ambient conditions, for more details refer to [37].

4. Results

In this section, the comparison between the thermal management systems is presented. At first, the dynamics of the two systems are analyzed on the WLTC taking into account a cabin conditioning targeted to 21 °C with an external ambient temperature of 35 °C. Afterwards, two cold conditions are considered for a cabin temperature of 20 °C (T_{ext} = -10, −20 °C) to highlight the strengths and weaknesses of the two systems. To conclude the WLTC analysis, the impact on the nominal driving range (i.e., measured at 24 °C) of the TMS activation is presented for both systems. Then, the impact of the battery preconditioning strategy on the driving range has been evaluated on the two lower external temperatures. During the preconditioning mode, the TMS is activated not only to guarantee the cabin thermal comfort but also to heat the battery to a safe temperature from the point of view of the battery operation and lifetime. The preconditioning strategy could be activated before or during the mission profile, if long enough. Two examples are here reported: preconditioning before the start of the mission for the shorter driving cycle (WLTC) and during the mission profile for the RDE driving cycle.

4.1. Systems dynamics and efficiency

In this paragraph, a comparison of the efficiency and performance of the systems is presented on the WLTC driving cycle considering only the cabin comfort conditioning. Fig. 6 compares the cabin temperature and compressor power as a function of time, with an external ambient temperature of 35 °C.

On the one hand, the standard TMS (blue lines) is characterized by a faster dynamic response. Indeed, thanks to the absence of an intermediate circuit for cabin conditioning, the target cabin air temperature is achieved in a shorter time with respect to the HP. (orange lines) On the other hand, in response to the HP system, the temperature initially increases since the high irradiance at this external ambient temperature is not yet counterbalanced by the heat exchange promoted by the HP activation. Regarding the compressor power, the standard AC system shows an oscillating behavior that is generated by the dependence on the mission profile: as a matter of fact, the higher the vehicle speed, the higher heat transfer thanks to the increased air mass flow rate available on the radiator and lower power requested by the compressor and by the blower. In addition, the standard AC system requires a lower compressor power with respect to the HP system, at steady-state. The presence of the indirect circuit for the HP configuration causes a higher compressor power request and less influence from the vehicle speed variation. From the energy consumption perspective, Fig. 7 presents a comparison of the two systems' efficiency in terms of COP, defined as:

$$COP = \frac{Q}{W}, \tag{1}$$

where Q is the useful effect to guarantee the thermal comfort in the cabin (i.e., cabin temperature T = 20 °C), and W is the work needed to move the refrigerant by the different components (compressor, blower, fan, and recirculation pump).

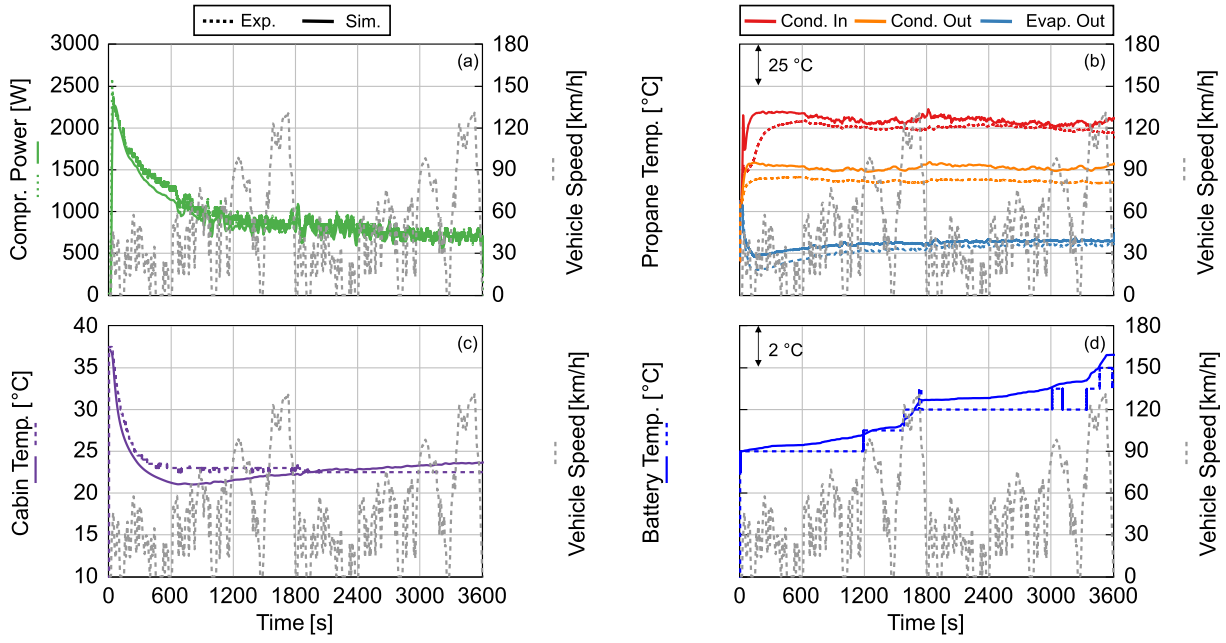

Fig. 5. HP model validation (solid lines) against experimental data (Dashed lines). Compressor power (a), propane temperature in the different CRU components (b), cabin temperature (c) battery temperature (d). The vehicle speed is represented in grey, for two consecutive WLTC driving cycles in hot external conditions.

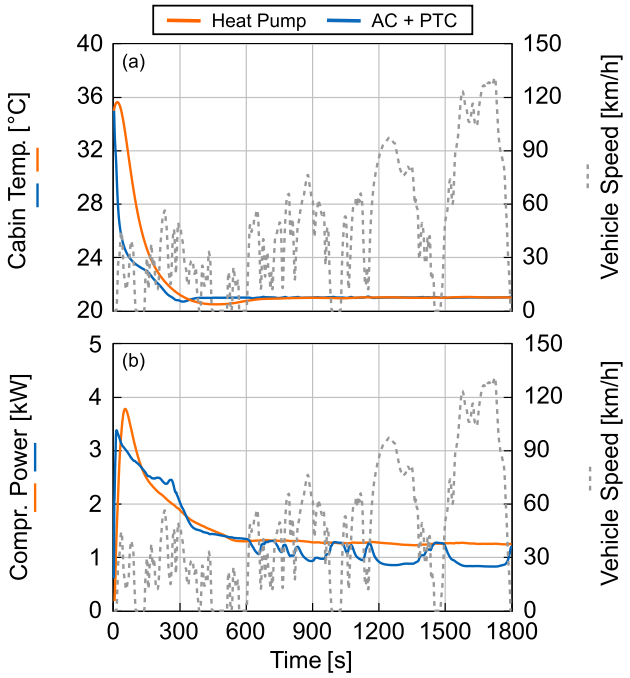

Fig. 6. Cabin temperature (a) and compressor power (b) as a function of time, the HP system (orange lines) and traditional TMS (blue lines), for an external ambient temperature of 35 °C. The vehicle speed is represented in grey, typical of a WLTC driving cycle.

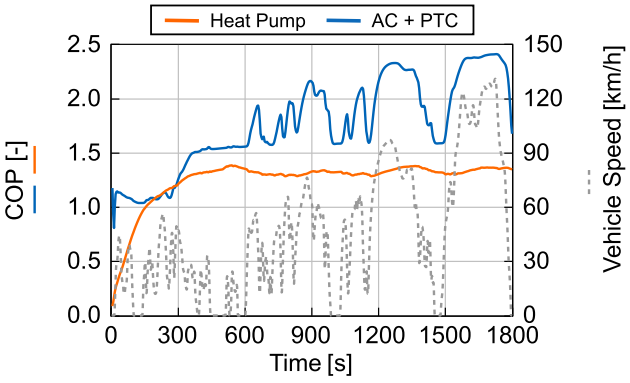

Fig. 7. COP for the HP system (orange line) and traditional TMS (blue line) for an external ambient temperature of 35 °C. The vehicle speed is represented in grey, typical of a WLTC driving cycle.

The COP calculated for the standard AC system with hot ambient conditions follows the same logic as the compressor power. The higher inertia of the HP affects the COP which is lower than 1 for the first 200 s of the mission profile. Therefore, the generated cold power is exploited in the early stages to cool down the intermediate refrigerant, which will subsequently reduce the cabin temperature. The COP of the HP is almost constant once the cabin temperature is reached since the indirect system is less influenced by the vehicle speed variation.

Moving to the cold external environment, Fig. 8 defines the evolution of the cabin temperature, considering an ambient temperature of −10 °C and −20 °C, respectively. A control strategy is actuated to avoid air at a temperature higher than 40 °C entering the cabin from the conditioning system, for passenger comfort constraints. The target temperature is reached almost at the same time by the two systems at $T_{ext} = -10$ °C, even if the response of the PTC system is faster with an increase almost immediately of the cabin air temperature of 15 °C. When the external ambient temperature is set to $T_{ext} = -20$ °C, the performance of the HP

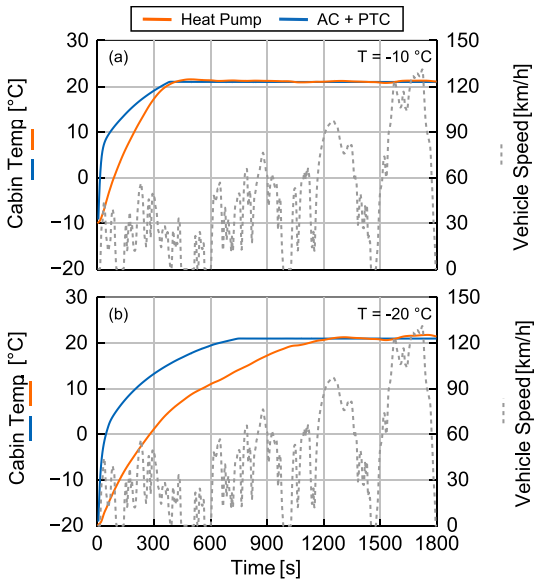

Fig. 8. Cabin temperature as a function of time, for the HP system (orange lines) and traditional TMS (blue lines), the external ambient temperature of T = −10 °C (a) and T = −20 °C (b). The vehicle speed is represented in grey, typical of a WLTC driving cycle.

is much slower, requiring about 20 min to achieve the target. On the contrary, the standard system can reach a cabin temperature of 15 °C in 5 min, while the fixed target is achieved after about 10 min of mission profile. In this case, the poor performance of the HP can be improved by adding a PTC to accelerate the cabin heating or considering a strategy of cabin preconditioning before the passenger occupancy.

Another interesting aspect in cold conditions for an indirect HP architecture is to partially recover heat from the powertrain and exploit it to heat the cabin. Recalling Fig. 2, the cold liquid of the secondary cycle after absorbing heat from the environment will pass through the powertrain components, before returning to the Heat Pump Unit. Exploiting the powertrain heat, the secondary liquid becomes hotter and will heat more the propane, allowing a faster heating of the cabin. During the present activity, only the feasibility of exploiting the powertrain heat was investigated and further improvements could be obtained by optimizing compressor and radiator fan actuation. The results of the present analysis are presented in Fig. 9, where the cabin temperature is represented as a function of time considering the powertrain as an additional heat source (full lines) or not (dotted lines). The considered mission profile is a WLTC driving cycle, performed forward (starting from the urban and ending with the highway segment) or backward (starting from the highway and ending with the urban segment). It emerges that in cold conditions, by exploiting the powertrain heat in the HP circuit (red full line), the cabin temperature reaches a higher value of 4 degrees at the end of the cycle, with respect to the case where the powertrain is bypassed in the HP circuit (red dotted line), with no penalty or gain in terms of SOC. At the same time, the effect is even more visible considering different mission profiles. In particular, if a highway segment with higher vehicle speeds and acceleration (backward WLTC, blue line) is performed at the beginning of the cruise, the rejected heat is significantly higher and this allows to heat the cabin faster with respect to the case where the urban segment is performed at the start of the mission (forward WLTC, red lines).

From the efficiency point of view, the average COP of the HP system has been calculated with four different external ambient temperatures, considering the heat delivered to the cabin as a useful effect (see Fig. 10). For the standard TMS, the COP of the PTC heater is by definition almost equal to one because the electricity needed by the component is converted into heat with an efficiency near 100 %. The HP

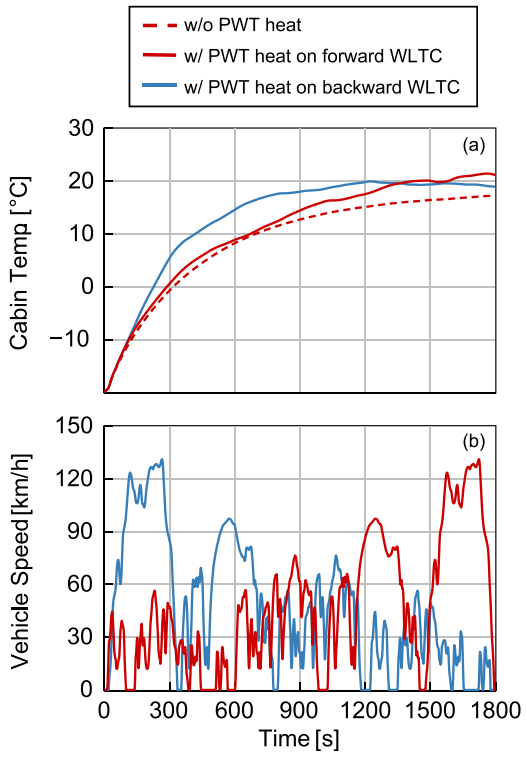

Fig. 9. (a) Cabin temperature as a function of time, for the HP system w/o exploiting powertrain heat (dotted line) and considering it (full lines), on a WLTC driving cycle performed forward (red lines) or backward (blue line). (b) Vehicle speed as a function of time, typical of a forward (red line) and backward (blue line) WLTC driving cycle.

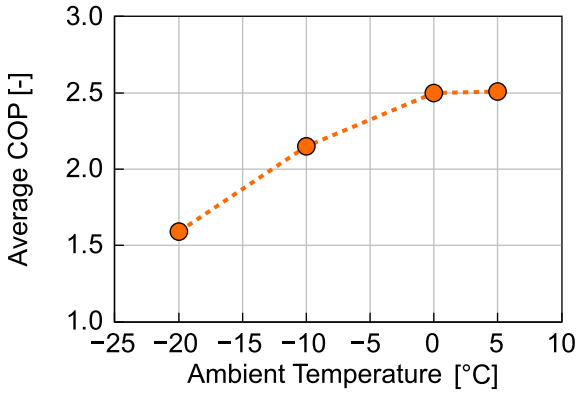

Fig. 10. Average COP of the HP system on a WLTC mission profile, considering different external ambient temperatures.

system obtains twice the efficiency of the PTC heater, except for $T_{ext} = -20$ °C where the performance of the HP is not satisfactory to guarantee cabin comfort.

This efficiency gains a positive impact on the vehicle range, as depicted in Fig. 11, where a summary of the driving range reduction is presented, calculated normalized with respect to the range declared by the manufacturer measured at 24 °C without cabin or battery conditioning.

Analyzing the extremely hot conditions ($T_{ext} = 42$ °C), the TMSs achieve similar performance, with a slight advantage over the standard AC system. The need for an indirect circuit for the HP plays a crucial role in the efficiency loss, causing a shorter driving range. Cold environments ($T_{ext} = -20, 5$ °C) are more favorable to the HP system, obtaining for the whole temperature sweep evident longer driving ranges, with respect to

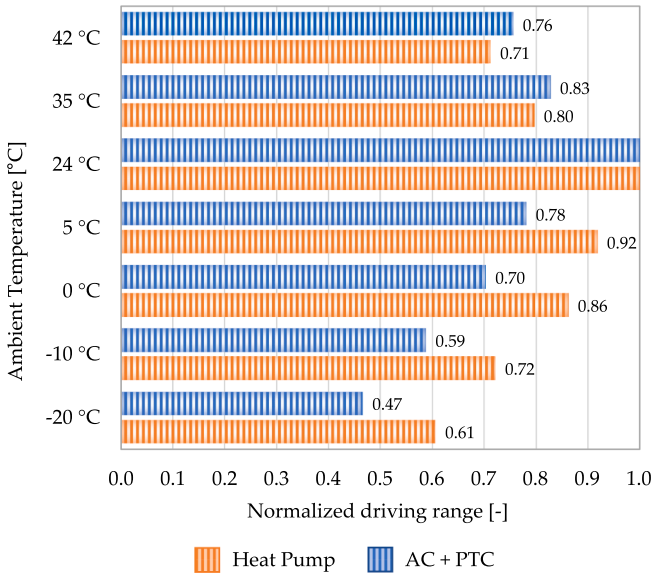

Fig. 11. Driving range at different external ambient temperatures with HP-based (orange bars) and standard (blue bars) TMS. Results normalized with respect to the full range at an external temperature of 24 °C with the TMS deactivated.

the ones granted by the standard TMS system. Indeed, as already described for the standard TMS, the heat required to condition the cabin in cold conditions is produced by the PTC, directly reducing the energy stored in the battery. It is worth mentioning that for the extreme cold conditions ($T_{ext} = -20$ °C) the cabin comfort is not comparable and, consequently, also the system performance (see Fig. 8b).

4.2. Battery preconditioning

In this paragraph, the results in terms of system efficiency and driving range are presented considering the activation of the TMS not only to guarantee cabin comfort but also the battery preconditioning, in case of cold external conditions. Indeed, with a range of temperature above 0 °C, the lower internal resistance of the battery guarantees better performance during the mission profile, and a longer battery lifetime, with lower risks of internal damage. As a consequence, the pre-conditioning strategy is activated on the two lower external ambient conditions ($T_{ext} = -20$ °C, −10 °C). In particular, the battery is heated to 0 °C, which is a good compromise between battery-safe operation, acceptable heating time, and energy consumption.

At first, a battery preconditioning before the start of the vehicle is applied to be compliant with the WLTC driving cycle: with a short mission profile, the battery preconditioning process is too long to be applied during the cruise. For $T_{ext} = -10$ °C the process of battery heating takes 20 min with the vehicle stopped to reach the battery target temperature, independently from the TMS configuration. Fig. 12 compares the evolution of the battery SOC together with the terminal current of the battery, obtained with and without battery preconditioning for the two TMS.

The initial SOC is lower when a preconditioning strategy is enabled with both systems because of the energy consumed to heat up the battery before the vehicle switches on. Nevertheless, the energy needed with the PTC is higher with respect to the one needed by the HP system due to the lower efficiency in cold conditions. Moreover, at the end of the mission, the SOC gap is completely recovered by the HP system (Fig. 12a), thanks to the lower internal resistance of the battery at higher temperatures. Indeed, as can be seen from the terminal current of the battery (Fig. 12c), the preconditioned battery can recover a higher amount of energy during the regenerative braking. On the contrary, for the

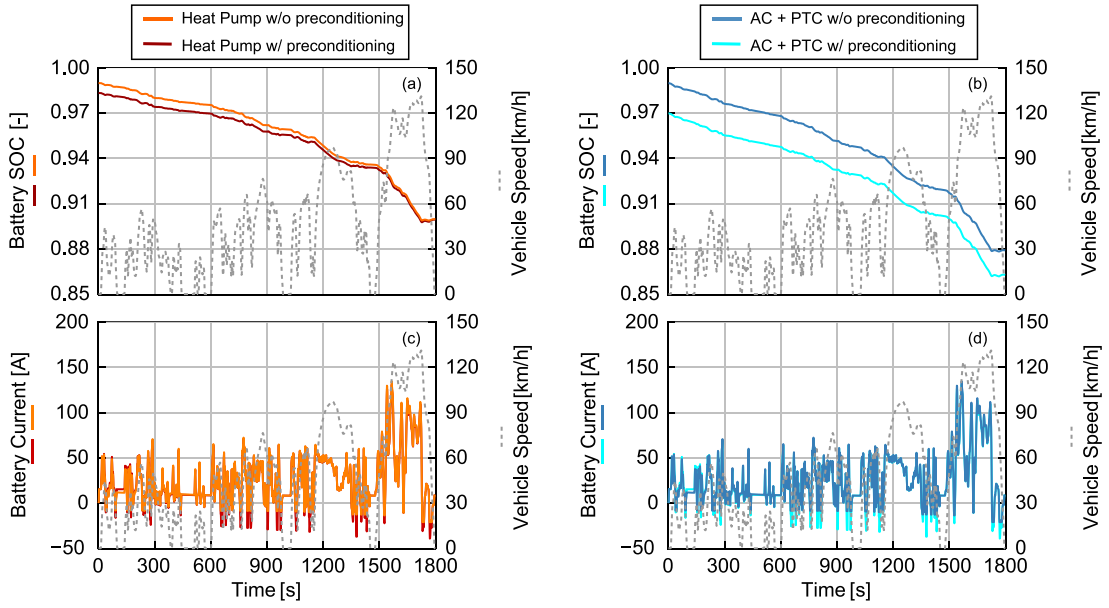

Fig. 12. Evolution of battery SOC (a,b) and battery terminal current (c,d) for the HP (a,c) and standard (b,d) TMS, with and without battery preconditioning, $T_{ext} = -10$ °C. The vehicle speed is represented in grey, typical of a WLTC driving cycle.

standard TMS, the trade-off between the battery lifetime and the driving range is more critical: as a matter of fact, the preconditioning strategy can keep the battery temperature in an acceptable range ($T > 0$ °C) to prevent failures, but, the penalty on the battery SOC during the mission profile is not negligible (Fig. 12b).

When a longer mission profile is considered (RDE driving cycle) the battery conditioning strategy can be enabled during cruising. The results in terms of battery SOC and temperature are presented in Fig. 13, together with the cabin temperature, with and without battery preconditioning strategy, for both TMSs. The TMS is activated at the start of the vehicle and a part of the heat produced during the cruise is devoted to the battery heating, with a penalty in the time needed to reach the cabin target temperature (see Fig. 13 c,d). In addition, in the initial part of the driving cycle, the battery is not kept at an optimal operating temperature, but this preconditioning strategy could be considered more comfortable for the driver, who is not forced to schedule a pre-activation of the TMS before the start of the vehicle.

The preconditioning is activated in the first part of the cycle and the battery target temperature is reached after 35 and 25 min employing the HP system (Fig. 13a, dashed red line) and the PTC heater (Fig. 13b, dashed cyan line), respectively. In the non-preconditioned case (Fig. 13a, orange dashed line) the heating process of the battery is slower, due to its high thermal inertia at lower temperatures. As a consequence, the non-preconditioned temperature profile of the battery

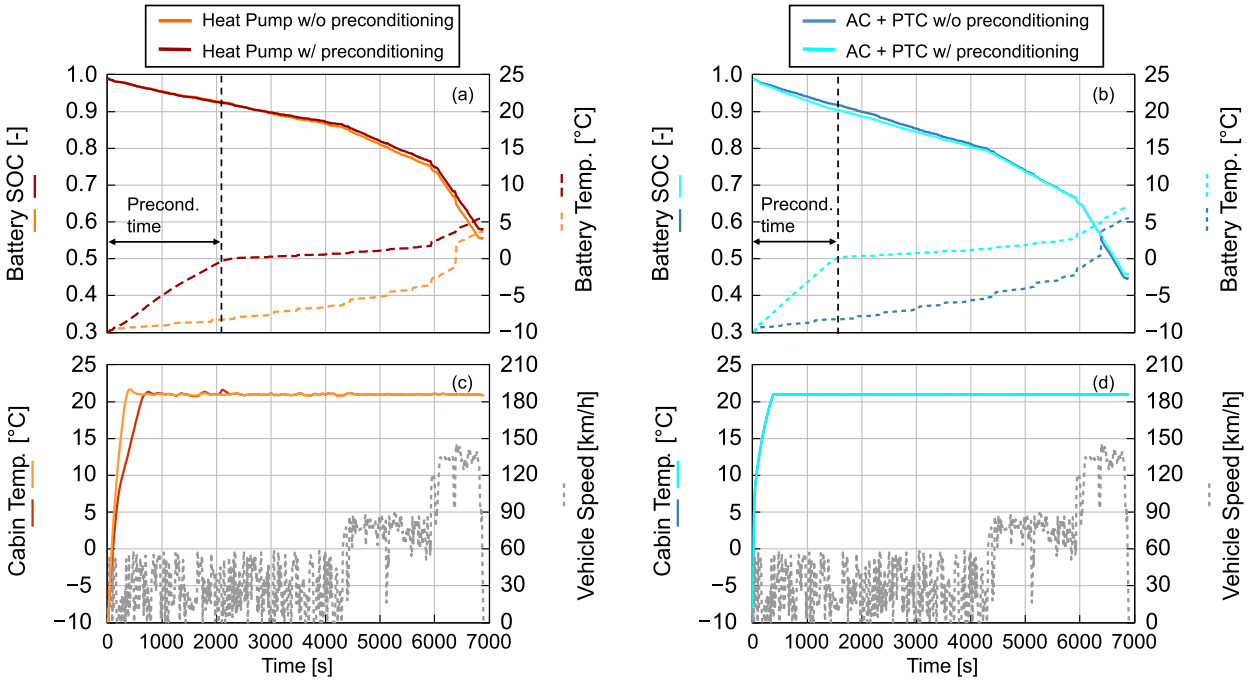

Fig. 13. Evolution of battery SOC, battery temperature (a,b), and cabin temperature (c,d) for the HP (a,c) and standard (b,d) TMS, with and without battery preconditioning, $T_{ext} = -10$ °C. The vehicle speed is represented in grey, typical of a RDE driving cycle.

lays for most of the driving cycle below 0 °C, which is a condition not favorable for battery performance and lifetime. From the cabin comfort perspective (Fig. 13c), in preconditioning mode, the total refrigerant power of the HP is split between battery and cabin circuits, reaching the target cabin temperature 4 min later in the driving cycle in comparison with respect to the non-preconditioned case. On the contrary, in the standard system (Fig. 13d) two different heaters for the cabin and the battery are present and, as a consequence, the preconditioning does not affect the time to achieve the cabin thermal target: the higher the thermal loads requested by the TMS, the higher the electricity consumed by the PTC heaters. Regarding the battery SOC, its initial value is set at the maximum in all the conditions, being the TMS deactivated before the vehicle starts. Until the battery heating is activated in the HP system the SOC is comparable to the non-preconditioned case, while in the second part of the mission, the better performance of the warmer battery becomes evident, with a final gain on the SOC of the 3 %. With the PTC configuration, the positive effect of the preconditioning strategy is less evident showing a negligible difference at the end of the mission profile. In addition, the SOC penalty is more evident during the battery heating phase, due to the higher electricity required by the two thermal loads (cabin and battery).

The effect of the battery preconditioning strategy on the driving range is highlighted in Fig. 14 and Fig. 15 for the WLTC and RDE, respectively, considering two different ambient temperatures. From the analysis of Fig. 14, it is evident that the preconditioning strategy results in a not negligible penalty in terms of range, when considering the PTC configuration (blue bars) (i.e., −12.7 %). Indeed, the gain in terms of battery efficiency during regenerative braking is not able to counterbalance the initial SOC loss due to the necessary energy to heat the battery before the mission. For the HP system (orange bars) with an external ambient temperature of T_{ext} = -10 °C, the final breakeven in terms of SOC guarantees a comparable driving range, while a further reduction of ambient temperature up to −20 °C produces a reduction of the driving range (i.e., −6.7 %), due to the higher energy required to raise the battery temperature of 20 °C and the difficulties in recovery the initial SOC on a short mission profile.

On the RDE (Fig. 15) the actuated battery conditioning strategy has positive impacts on the driving range. The HP system (orange bars), at all ambient temperatures, achieves an improvement of 5–6 %, thanks to the higher efficiency and the longer time for the mission available to recover the SOC loss due to the battery heating. For the standard configuration with the PTC heater (blue bars), the beneficial effect of the longer mission profile develops in a comparable driving range for the different cold ambient conditions.

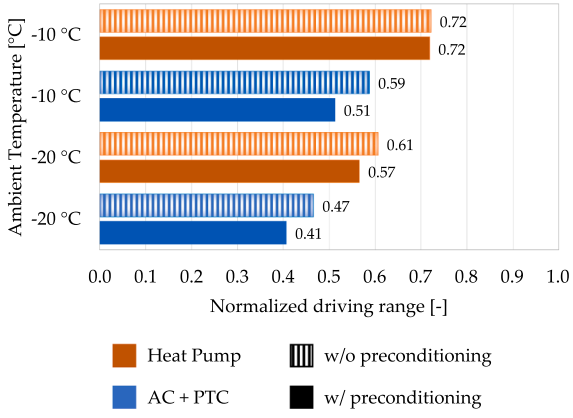

Fig. 14. Driving range on the WLTC at different external ambient temperatures with HP-based (orange bars) and standard (blue bars) TMS, w/o preconditioning strategy (striped bar), w/ preconditioning (plain color).

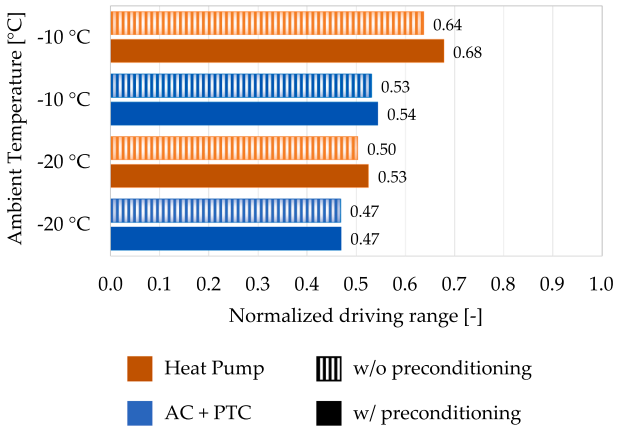

Fig. 15. Driving range on the RDE at different external ambient temperatures with HP-based (orange bars) and standard (blue bars) TMS, w/o preconditioning strategy (striped bar), w/ preconditioning (plain color).

5. Conclusions

In the present work, a virtual test rig has been developed to compare the performance of different Thermal Management Systems (TMSs) of a Battery Electric Vehicle (BEV), in a wide range of environmental conditions. The efficiency and performance of an innovative indirect Heat Pump (HP) system based on propane refrigerant have been tested in real driving conditions, evaluating the impact on the driving range and on the cabin conditioning, as one of the first examples in the literature. Minor penalties have been obtained on the driving range in warm conditions with respect to a traditional Air Conditioning (AC) system, based on a direct cycle of R134a. Moderate cold external conditions are more favorable to the HP system with respect to a traditional TMS featuring two PTC heaters, showing a gain of 20–25 % in the driving range, and suggesting propane as a competitive alternative among the different low GWP refrigerants. In addition, the future steps of the work will include a performance analysis of a TMS system based on a direct CO_2 HP.

The use of the battery preconditioning strategy has also been tested, not only to enhance the performance of the battery during the mission but also to safeguard its lifetime. At first, the effect of battery preconditioning before the start of the vehicle has been tested with the HP system in the presence of short cycles. Then, benefits in terms of gained drive range have been obtained on longer mission profiles, with the integration of battery heating during the cycle (i.e., +6% at −10 °C). Finally, the developed physical model could be further employed to analyze other critical situations that need battery conditioning, such as the recharging process, paving the way to fast charging strategies.

Funding

The activity has been partially financed by the European Union – Next Generation EU - PNRR M4C2, Investimento 1.4 - Avviso n. 3138 del 16/12/2021 - CN00000023 Sustainable Mobility Center (Centro Nazionale per la Mobilita` Sostenibile) - CNMS - CUP E13C22000980001.

CRediT authorship contribution statement

Federico Millo: Writing – review & editing, Supervision, Project administration, Conceptualization. **Luciano Rolando:** Writing – review & editing, Validation, Methodology, Investigation, Formal analysis. **Afanasie Vinogradov:** Writing – original draft, Validation, Methodology, Investigation, Formal analysis. **Benedetta Peiretti Paradisi:** Writing – original draft, Methodology, Investigation, Formal analysis. **Alessandro Allocco:** Writing – review & editing, Supervision, Project administration, Conceptualization. **Pasquale Ceres:** Writing – review &

editing, Supervision, Project administration, Conceptualization. **Rossella Marco:** Writing – review & editing, Supervision, Project administration, Conceptualization. **Matteo Maria Rostagno:** Writing – review & editing, Supervision, Project administration, Conceptualization.

Declaration of competing interest

The authors declare that they have no known competing financial interests or personal relationships that could have appeared to influence the work reported in this paper.

Data availability

The data that has been used is confidential.

References

[1] International Energy Agency. Global EV Outlook 2023: Catching up with climate ambitions, 2023.

[2] P. Chakraborty, R. Parker, T. Hoque, J. Cruz, L. Du, S. Wang, S. Bhunia, Addressing the range anxiety of battery electric vehicles with charging en route, Sci. Rep. 12 (1) (2022), https://doi.org/10.1038/s41598-022-08942-2.

[3] S. Bellocchi, G. Leo Guizzi, M. Manno, M. Salvatori, A. Zaccagnini, Reversible heat pump HVAC system with regenerative heat exchanger for electric vehicles: analysis of its impact on driving range, Appl. Therm. Eng. 129 (2018) 290–305, https://doi.org/10.1016/j.applthermaleng.2017.10.020.

[4] J. Zhan, Y. Deng, Y. Gao, J. Ren, Y. Liu, S. Rao, W. Li, Z. Gao, Y. Chen, A review on low-temperature performance management of lithium-ion batteries, J. Electrochem. Energy Convers. Storage 21 (3) (2024), https://doi.org/10.1115/1.4063611.

[5] T.M. Bandhauer, S. Garimella, T.F. Fuller, A critical review of thermal issues in lithium-ion batteries, J. Electrochem. Soc 158 (3) (2011) R1, https://doi.org/10.1149/1.3515880.

[6] Z. Zhang, J. Wang, X. Feng, L. Chang, Y. Chen, X. Wang, The solutions to electric vehicle air conditioning systems: a review, Renew. Sustain. Energy. Rev. 91 (2018) 443–463, https://doi.org/10.1016/j.rser.2018.04.005.

[7] Y. Higuchi, H. Kobayashi, Z. Shan, M. Kuwahara, Y. Endo, Y. Nakajima, Efficient heat pump system for PHEV/BEV, SAE Technical Papers 2017-01-0188 (2017), https://doi.org/10.4271/2017-01-0188.

[8] D. Wu, B. Hu, R.Z. Wang, Vapor compression heat pumps with pure low-GWP refrigerants, Renew. Sustain. Energy Rev. 138 (2021), https://doi.org/10.1016/j.rser.2020.110571.

[9] http://www.nissan-global.com/EN/TECHNOLOGY/OVERVIEW/heat pump cabin heater.html, "Nissan LEAF Heat-Pump Cabin Heater.".

[10] https://www.volkswagen.co.uk/en/electric-and-hybrid/software-and-technology/id-technology/heat-pump.html, "ID.3 and ID.4 Volkswagen.".

[11] https://www.tesla.com/it_it/modely, "Tesla Model Y.".

[12] D. Lee, Experimental study on the heat pump system using R134a refrigerant for zero-emission vehicles, Int. J. Automot. Technol. 16 (6) (2015) 923–928, https://doi.org/10.1007/s12239−015−0094−2.

[13] H. Lee, D. Lee, Y. Kim, Heating performance of a coolant-source heat pump using waste heat from stack and electric devices in fuel cell electric vehicles under cold conditions, Energy. Convers. Manag 252 (2022), https://doi.org/10.1016/j.enconman.2021.115092.

[14] W. Li, R. Liu, Y. Liu, D. Wang, J. Shi, J. Chen, Performance evaluation of R1234yf heat pump system for an electric vehicle in cold climate, Int. J. Refrigerat. 115 (2020) 117–125, https://doi.org/10.1016/j.ijrefrig.2020.02.021.

[15] S. Lee, Y. Chung, S. Kim, Y. Jeong, M.S. Kim, Predictive optimization method for the waste heat recovery strategy in an electric vehicle heat pump system, Appl. Energy 333 (2023), https://doi.org/10.1016/j.apenergy.2022.120572.

[16] H. Zou, B. Jiang, Q. Wang, C. Tian, Y. Yan, Performance analysis of a heat pump air conditioning system coupling with battery cooling for electric vehicles, Energy Procedia 891–894 (2014), https://doi.org/10.1016/j.egypro.2014.11.989.

[17] H. Rezaei, M.J. Ghomsheh, F. Kowsary, P. Ahmadi, Performance assessment of a range-extended electric vehicle under real driving conditions using novel PCM-based HVAC system, Sustain. Energy Technol. Assessments 47 (2021), https://doi.org/10.1016/j.seta.2021.101527.

[18] J. Jeffs, A. McGordon, W.D. Widanage, S. Robinson, A. Picarelli, Use of a thermal battery with a heat pump for low temperature electric vehicle operation, in: IEEE Vehicle Power and Propulsion Conference (VPPC), 2017, https://doi.org/10.1109/VPPC.2017.8330932.

[19] J. Kim, J. Oh, H. Lee, Review on battery thermal management system for electric vehicles, Appl. Therm. Eng 149 (2019) 192–212, https://doi.org/10.1016/j.applthermaleng.2018.12.020.

[20] European Parliament (EUROPA), Regulation (EC) No. 842/2006 of the European Parliament and of the Council of 17 on certain fluorinated greenhouse gases, Off. J. Eur. Union 2006 (L161) (May 2006) 1–11.

[21] J. Wu, G. Zhou, M. Wang, A comprehensive assessment of refrigerants for cabin heating and cooling on electric vehicles, Appl. Therm. Eng 174 (2020), https://doi.org/10.1016/j.applthermaleng.2020.115258.

[22] S. Daviran, A. Kasaeian, S. Golzari, O. Mahian, S. Nasirivatan, S. Wongwises, A comparative study on the performance of HFO-1234yf and HFC-134a as an alternative in automotive air conditioning systems, Appl. Therm. Eng 110 (2017) 1091–1100, https://doi.org/10.1016/j.applthermaleng.2016.09.034.

[23] D. Wang, B. Yu, J. Hu, L. Chen, J. Shi, J. Chen, Heating performance characteristics of CO2 heat pump system for electrical vehicle in a cold climate, International. Journal. of. Refrigeration 85 (2018) 27–41, https://doi.org/10.1016/j.ijrefrig.2017.09.009.

[24] Y. Huang, X. Wu, J. Jing, Research on the electric vehicle heat pump air conditioning system based on R290 refrigerant, Energy. Reports 8 (2022) 447–455, https://doi.org/10.1016/j.egyr.2022.05.112.

[25] C. Liu, Y. Zhang, T. Gao, J. Shi, J. Chen, T. Wang, L. Pan, Performance evaluation of propane heat pump system for electric vehicle in cold climate, Int. J. Refrigerat. 95 (2018) 51–60, https://doi.org/10.1016/j.ijrefrig.2018.08.020.

[26] H. Wang, Z. Ji, C. Wang, Z. Zhu, Y. Wang, H. Lin, Experimental study of propane heat pump system with secondary loop and vapor injection for electric vehicle application in cold climate, Appl. Therm. Eng 217 (2022), https://doi.org/10.1016/j.applthermaleng.2022.119196.

[27] A. Broatch, P. Olmeda, B. Plá, A. Dreif, A. Onorati, A. Marinoni, Numerical assessment of integrated thermal management systems in electrified powertrains, Appl. Therm. Eng 221 (2023), https://doi.org/10.1016/j.applthermaleng.2022.119822.

[28] G. Titov, J.A. Lustbader, Modeling control strategies and range impacts for electric vehicle integrated thermal Management systems with MATLAB/Simulink, SAE technical papers 2017-01-0191 (2017), https://doi.org/10.4271/2017-01-0191.

[29] K. Li, J. Wang, S. Luo, Z. Wang, X. Zhou, J. Fang, L. Su, R. Tu, Experimental investigation on combustion characteristics of flammable refrigerant R290/R1234yf leakage from heat pump system for electric vehicles, R Soc. Open. Sci. 7 (4) (2020), https://doi.org/10.1098/rsos.191478.

[30] J. Jeffs, A. McGordon, A. Picarelli, S. Robinson, W.D. Widanage, in: System level heat pump model for investigations into thermal management of electric vehicles at low temperatures, Proceedings of the 13th International Modelica Conference, Regensburg, Germany, March 4–6,, University Electronic Press, Linköing, 2019, pp. 107–116, https://doi.org/10.3384/ecp19157107.

[31] L. Pulvirenti, L. Rolando, F. Millo, Energy management system optimization based on an LSTM deep learning model using vehicle speed prediction, Transport. Eng. 11 (2023), https://doi.org/10.1016/j.treng.2023.100160.

[32] Gamma Technologies, GT SUITE User Manual, (2022).

[33] F. Millo, L. Rolando, M. Andreata, Numerical simulation for vehicle powertrain development, Numerical Analysis-Theory and Application, IntechOpen, 2011.

[34] G.L. Plett, Battery management systems, Volume I: Battery modeling. Vol. 1., 2015.

[35] G. De Nunzio, A. Sciarretta, A. Steiner, A. Mladek, Thermal management optimization of a heat-pump-based HVAC system for cabin conditioning in electric vehicles, in: 2018 13th International Conference on Ecological Vehicles and Renewable Energies, EVER 2018, 1–7, 2018, https://doi.org/10.1109/EVER.2018.8362408.

[36] W. Li, Simplified steady-state modeling for variable speed compressor, Appl. Therm. Eng. 318–326 (2013), https://doi.org/10.1016/j.applthermaleng.2012.08.041.

[37] F. Millo, L. Rolando, A. Vinogradov, B. Peiretti Paradisi, D. Regruto, Development of a virtual test rig for advanced thermal management system for battery electric vehicles, GT. Tech. Conf. (2022).